Millimeter-Wave Circularly Polarized Array Antenna Using Substrate-Integrated Gap Waveguide Sequentially Rotating Phase Feed

Chaojun Ma, Zu-Hui Ma, *Member, IEEE*, and Xiupu Zhang, *Senior Member, IEEE*

***Abstract*—A substrate-integrated gap waveguide (SIGW) sequentially rotating phase (SRP)-fed 2 × 2 circularly polarized (CP) patch antenna array is presented for the wideband millimeter-wave application. The antenna element is composed of a truncated square patch, SIGW feedline with three layers of printed circuit board (PCB), and another layer of PCB with an air hole for supporting radiation patch. Each radiation patch is driven by an underneath coupling slot etched on SIGW. A wide axial-ratio (AR) bandwidth is achieved by deploying a 2 × 2 SIGW SRP feed network. Moreover, simple calculation expressions of the characteristic impedance and guide wavelength of SIGW are given for the design of SRP feed network. The fabricated prototype shows an impedance bandwidth of 25.6% covering 22.2–28.8 GHz, 3 dB AR bandwidth of 19% from 22.8 to 27.6 GHz, and peak gain of 11.53 dBic.**

***Index Terms*—Antenna array, circularly polarized (CP), millimeter-wave (MMW), substrate integrated gap waveguide (SIGW).**

I. Introduction

CIRCULARLY polarized (CP) antennas have been widely investigated and used in many wireless applications such as satellite communication systems, radar, and high-resolution sensors. With increasing interests toward 5G millimeter-wave (MMW) applications, high-gain and wideband CP antenna array are preferred to overcome the propagation attenuation and support high-data-rate transmission as well.

The sequentially rotating phase (SRP) feed is a popular method in the CP antenna array design, which has been utilized for improving the bandwidth and polarization purity [1]. The SRP has been not only successfully exploited for low-frequency applications [2], [3], but also employed in MMW CP antenna array designs. For example, several kinds of SRP CP antenna arrays with different feed technologies for MMW applications were presented in [4]–[11], including microstrip line (MSL) on printed circuit board (PCB) [4], low-temperature cofired ceramics (LTCC) [5], [6], substrate integrated waveguide (SIW) [7]–[9], and fully metallic ridge-gap waveguide (RGW) [10]. However, these technologies have some shortages to meet the demand of MMW wireless communication systems. The MSL-based structures are convenient to design, but they often suffer from poor line-to-line isolation and radiation leakage due to their open structures, especially in highly integrated MMW applications. The SIW is able to provide an excellent shielding performance, but its dimension is limited severely by the cutoff wavelength. Consequently, the multilayer coupling method [7], [9] is commonly employed in SIW SPR feed network, though it is accompanied with additional losses and efficiency reduction. On the other hand, the RGW [10] could be applied only for feeding subarrays; it cannot serve as radiation elements. As a result, the array scale will be limited by using such technology.

More recently, the substrate-integrated gap waveguide (SIGW) has been developed [11], [12] to improve the above problems, which completely packages a microstrip-via-hole ridge or a strip line, using perfect electric conductor (PEC) and perfect magnetic conductor (PMC). Thanks to the electromagnetic band gap (EBG) characteristic in between PEC and PMC, electromagnetic waves are only allowed propagating along the microstrip-via hole ridge or strip line locally, and prohibited in other regions. Compared with conventional MSL, SIGW has superior shielding performance to reduce the mutual coupling and leaky losses. Moreover, for the array design, SIGW has more compact configuration than SIW, which is flexible to construct complex array without increasing layers. In addition, the SIGW supports quasi-TEM modes, so that it can be integrated with other planner circuits without mode conversion.

Although these kinds of novel structures were then successfully utilized in some single-antenna applications [13], [14], they have yet to be employed to the CP array antenna design for 5G MMW applications. In this letter, we propose a 2 × 2 CP slot-coupling antenna array using SIGW SRP feed network. Each antenna element achieves the SRP by adding phase-delay lines with different length. For facilitating the SIGW SRP feed network design, an approximate calculation of the initial value of characteristic impedance and guide-wave wavelength is investigated. A prototype of the proposed antenna array is fabricated and measured for the validation purpose.

II. Antenna Element Design

The overall configuration of the proposed circular polarized antenna unit is shown in Fig. 1. It is composed of five PCBs: The lower three layers (1#,2# and 3#) form SIGW; the upper PCB (5#) is printed with a truncated-corner square patch as a radiation element; and the middle one (4#) with a drilled hole is used to

Manuscript received February 28, 2019; revised March 29, 2019; accepted April 5, 2019. Date of publication April 11, 2019; date of current version May 31, 2019. This work was supported in part by the National Science Foundation of China under Grant 61501398 and in part by the Open Foundation of State Key Laboratory of Millimeter Waves under Grant K201618. *(Corresponding author: Zu-Hui Ma.)*

C. Ma and Z.-H. Ma, are with the School of Information Science and Engineering, Yunnan University, Yunnan 650221, China (e-mail: chjma37@163.com; mazuhui@ynu.edu.cn).

X. Zhang is with the iPhotonics Labs, Department of Electrical and Computer Engineering, Concordia University, Montreal, QC H3G1M8, Canada (e-mail: xzhang@ece.concordia.ca).

Digital Object Identifier 10.1109/LAWP.2019.2910657

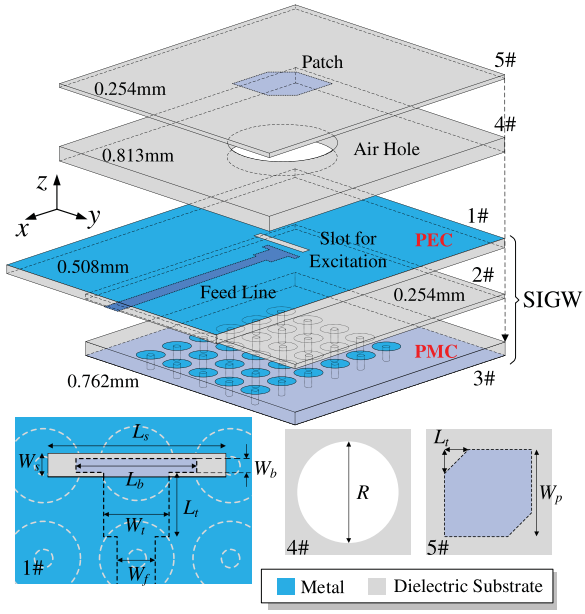

Fig. 1. Configuration of proposed CP antenna element ($L_t = 1.1$ mm, $L_s = 3.8$ mm, $L_b = 2.5$ mm, $L_t = 1.3$ mm, $W_p = 3.9$ mm, $W_s = 0.5$ mm, $W_b = 0.4$ mm, $W_t = 1.4$ mm, $W_f = 0.8$ mm, $R = 6$ mm).

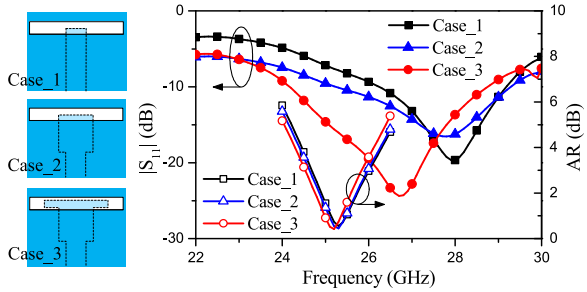

Fig. 2. Simulated $|S_{11}|$ results for three microstrip transitions under the coupling slot.

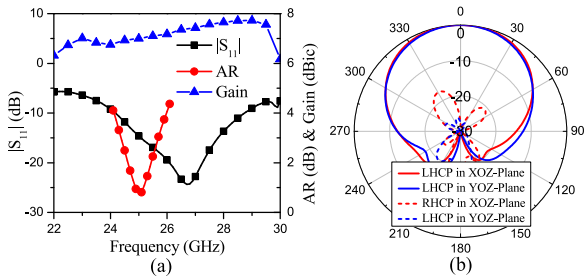

Fig. 3. Simulated results of the proposed antenna element in (a) $|S_{11}|$, AR, and gain. (b) Radiation pattern at 25 GHz.

support the radiation element. The PCBs 1#, 2#, 3#, and 5# are based on Rogers 4350 with $\varepsilon_r = 3.48$ and $\tan\delta = 0.0037$, while PCB 4# uses the substrate of Rogers 4003C with $\varepsilon_r = 3.38$ and $\tan\delta = 0.0027$. Moreover, thicknesses of substrates are shown in Fig. 1.

The bottom part, including PCBs 1#, 2#, and 3#, is the SIGW feed structure, and the working principle and design procedure of the SIGW can be found in [12]. The PCB 1# is printed with MSLs on the bottom side and a PEC layer as the ground on the other side. The PCB 3# works as a PMC layer, in which a grounded mushroom-shaped periodic structure array with 2 mm period is deployed; and each mushroom-shaped structure is composed of a circular patch with 1.5 mm diameter and a via hole with 0.4 mm diameter. In addition, the PCB 2# is utilized for separating electric contacts between PCBs 1# and 3#. With this configuration, the EBG effect is generated between the PEC and PMC, and the resulting electromagnetic wave is only able to propagate along the trace of the inner strip line.

As printed on the bottom side of PCB 5# for the anticorrosion purpose, the radiation element is designed as a truncated square with dimension of $W_p \times W_p$ ($0.34\lambda \times 0.34\lambda$, λ is the free-space wavelength at 26 GHz) so that two orthogonal resonance modes with 90° phase difference can be excited. In order to excite this radiation element, a rectangular slot of $L_s \times W_s$ ($0.33\lambda \times 0.04\lambda$) is etched on the exterior side of PCB 1#, i.e., the PEC layer. The inner MSL extends to the position under the slot for coupling signal. However, the bare use of an MSL without additional transformer or matching branch results in a poor performance, as illustrated in Fig. 2, in which three different transition schemes are simulated: Case_1 represents MSL only, Case_2 is the MSL with a rectangular impedance transformer, and Case_3 considers a MSL with a T-shaped impedance transformer. It can be observed that Case_3 is the best choice because it results in the widest -10 dB impedance bandwidth and the lowest resonance frequency. The simulated results show that Case_1 and Case_2 have little influence on AR resonant frequency and AR bandwidth. In Case_3, the AR frequency band is slightly shifted to lower frequency by 0.1 GHz. Because PCB 5# is quite thin, PCB 4# is introduced as a support layer to prevent deformation in practice. Since the dielectric substrate has higher permittivity and loss than air, it brings about a high Q-factor. However, because a low Q-factor is needed for wideband antennas [15], an air hole is drilled on PCB #4 to meet the demand of antenna performance and assembling.

The proposed antenna element is simulated in ANSYS HFSS, and the results of $|S_{11}|$, axial ratio (AR), and peak gain are shown in Fig. 3(a). It can be found that the -10 dB impedance bandwidth is $\sim$17% covering 24.2–28.7 GHz, the 3 dB AR bandwidth is $\sim$5.2% from 24.4 to 25.7 GHz, and the gain over 7 dBic in these above frequency band. Fig. 3(b) shows that left-hand (LH) CP radiation is predominant in *xoz* and *yoz* plane at 25 GHz. In addition, a lower backlobe level can be obtained by using SIGW feed, which is beneficial to gain enhancement.

III. Antenna Array Design

In order to improve the AR bandwidth of the aforementioned single-element antenna, an SRP feed network that is realized by an out-of-phase four-way power divider with additional phase-delay lines is used for building antenna array. To this end, an estimation method is given to calculate the characteristic impedance and guide wavelength to facilitate design and optimization.

A. Characteristic Impedance

Because the electric field is almost restricted in the region between the inner MSL and PEC layer [13], SIGW can be locally regarded as an MSL with dielectric fill in the surrounding space if the three PCB layers of the SIGW are with the same

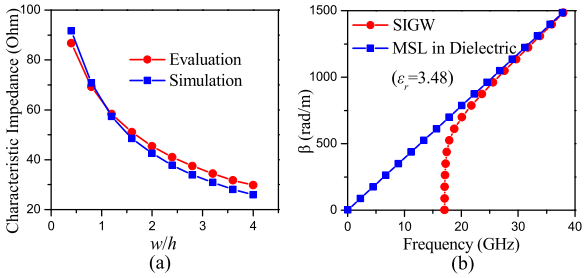

Fig. 4. Characteristic parameters of SIGW. (a) Calculated and simulated characteristic impedances versus different *w*/*h*. (b) Simulated phase constant of SIGW and MSL embedded in dielectric with ε_r of 3.48.

relative permittivity ε_r. Therefore, the characteristic impedance of SIGW Z_{SIGW} is able to be evaluated using the method for the conventional MSL by replacing the effective permittivity ε_e with ε_r. In this way, an equation related to Z_{SIGW} and Z_{MSL} under the same *w*/*h* is established as follows:

$$Z_{\mathrm{SIGW}} \cong \sqrt{\frac{\varepsilon_e}{\varepsilon_r}} Z_{\mathrm{MSL}} \tag{1}$$

where Z_{MSL} is the characteristic impedance of conventional MSL and *w* and *h* represent the width of MSL and height from MSL to its ground, respectively. In practice, Z_{MSL} can be calculated easily by solving an equation or using software tools, for instance, ADS Linecalc, when *w*/*h* and ε_e are given. Conversely, we can also do the synthesis for *w*/*h* when Z_{SIGW} is fixed. Evaluated and simulated characteristic impedance for different widths of MSL of SIGW are plotted in Fig. 4(a), where *h* is fixed as 0.508 mm. It can be seen that the difference between evaluated and simulated is less than 4 Ω in the range of $0.4 \leq w/h \leq 4$.

B. Guide Wavelength

Since the guide wavelength of a transmission line can be derived from its phase constant, we investigate phase constants of SIGW (β_{SIGW}) and MSL (β_{MSL}) with the same dielectric fill. As shown in Fig. 4(b), within the working frequency band of SIGW, β_{SIGW} is very close to β_{MSL}. Therefore, the initial guide wavelength of SIGW λ_{SIGW} can be reasonably evaluated using

$$\lambda_{\mathrm{SIGW}} = \frac{2\pi}{\beta_{\mathrm{SIGW}}} \cong \frac{2\pi}{\beta_{\mathrm{MSL}}} = \frac{c}{\sqrt{\varepsilon_r} f} \tag{2}$$

where *c* is the light velocity in free space, ε_r denotes relative permittivity of filling dielectric, and *f* is the frequency.

C. SRP Feed Network

Employing the aforementioned method to calculate the characteristic impedance and the guide wavelength of SIGW, we propose an SRP network for feeding the antenna array. The schematic and layout of this SRP feed network are shown in Fig. 5. The center-to-center distance of adjacent antenna elements is chosen as 10 mm (0.86λ) for a tradeoff between gain and sidelobe level. By adding phase-delay line with different electric lengths, the desired rotated phase for each element can be achieved. In this design, the widths of MSL in SIGW for 50 Ω and 100 Ω characteristic impedance are determined as 0.8 and 0.18 mm, respectively, and the guide wavelength is 5.6 mm.

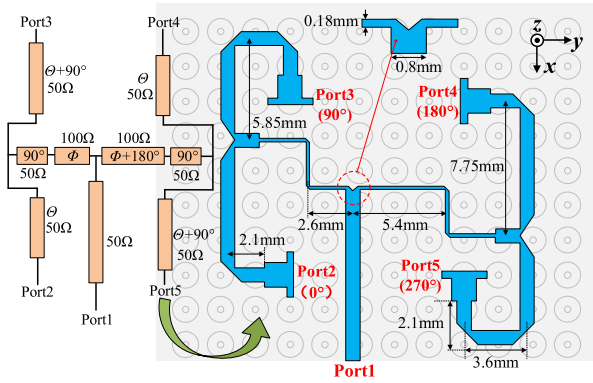

Fig. 5. Schematic and layout of the proposed SPR feed network.

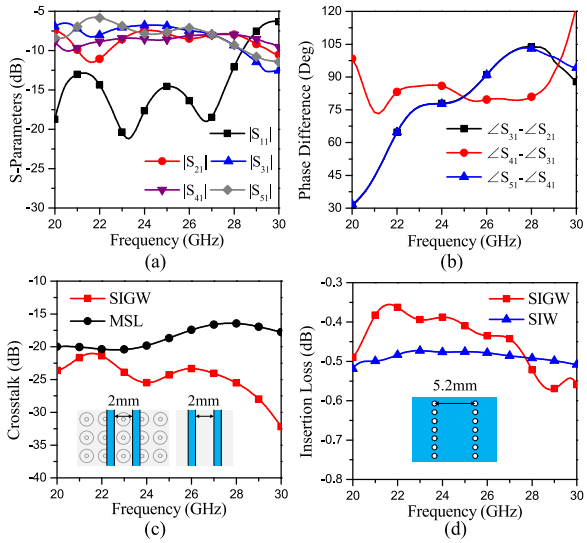

Fig. 6. Simulated results of SIGW feed network. (a) *S*-parameter. (b) Phase difference of four output ports. (c) Crosstalk level comparison of SIGW and MSL with adjacent length of 2 mm. (d) Insertion loss comparison of SIGW and SIW with physical length of 20 mm.

Simulated results of this SPR feed network are shown in Fig. 6(a) and (b): Within 23–28 GHz, the mean magnitude of transmission coefficients is −7.8 dB, the fluctuation is lower than 1.7 dB, and the error of phase difference in four output ports is lower than 15°. Moreover, the crosstalk levels and loss are investigated. Fig. 6(c) shows a comparison of the crosstalk between a pair of parallel strip lines in SIGW and two MSLs. As can be seen, within the frequency band from 20 to 30 GHz, the SIGW leads to crosstalk level of lower than −20 dB, while the conventional MSL results in crosstalk level larger than −20 dB. Fig. 6(d) plots the simulated insertion loss of SIGW and SIW with length of 20 mm. Furthermore, SIGW has lower insertion loss (<0.5 dB) than SIW within 20–27.8 GHz. Larger than 27.8 GHz, the insertion loss of SIGW increases because it approaches the upper cutoff frequency of EBG.

D. SRP Array Performance

In order to validate the proposed 2 × 2 antenna array, a prototype was fabricated and also measured. The photographs of the

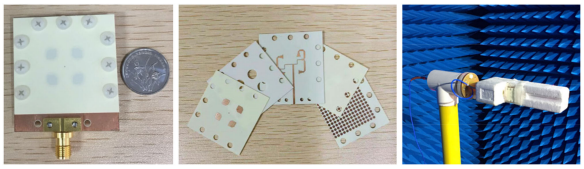

Fig. 7. Photograph of antenna array prototype and testing environment.

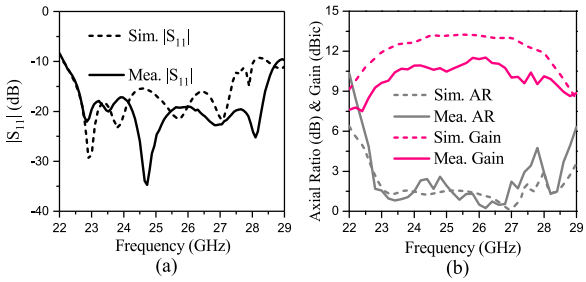

Fig. 8. Measured and simulated (a) $|S_{11}|$ and (b) AR and gain.

prototype and the testing environment are shown in Fig. 7. Moreover, the overall size of the prototype is $45 \times 40 \times 2.591$ mm^3 (coaxial connector is not included).

Fig. 8(a) plots the measured $|S_{11}|$, which is compared to simulated data. As can be seen, the measured -10 dB impedance bandwidth is from 22.2 to 28.8 GHz (25.6%), while the simulated one is from 22.2 to 28 GHz (23.1%). Moreover, measured and simulated AR and gain are plotted in Fig. 8(b). The measured 3 dB AR bandwidth is 19%, from 22.8 to 27.6 GHz, while the simulated one is 23.3%, from 22.8 to 28.8 GHz. In this 3 dB AR frequency band, the measured average gain of 10.6 dBic and peak gain of 11.53 dBic are obtained, whereas the simulated average gain and peak gain are 12.57 and 13.24 dBic, respectively. The difference between the simulated and measured gain mainly ascribes to the following factors:

1) For the measurement purpose, a 2.92 coaxial connector and a 2.92-to-2.4 adaptor are used, leading to an additional connection loss, which is not taken account in simulations.
2) This multilayer design is assembled by tightening screws, so a paper-thin air gap is inevitable to exist in the interfaces of two PCBs, which induces gain deteriorating [7].
3) Alignment mismatch of far-field measurement system would cause the reduction of reception level.

The normalized CP radiation patterns of the array at 23, 25, and 27 GHz are illustrated in Fig. 9. The measured and simulated results agree well in the broadside direction.

A comparison with recently reported SPR CP array antennas is summarized in Table I. The proposed array has comparable bandwidth in impedance and AR. Moreover, compared to microstrip-based CP array [4], [5], the proposed array has superior shielding performance without the need of additional packages. In contrast with SIW CP arrays [9], the proposed one has more compact circuit configuration, and it will not increase the number of layers when designing large or complex arrays. Additionally, the utilized SIGW elevates the signal line from the PMC layer with periodic structures by using a separate layer. This design makes circuit layout of SIGW free from the limitation of periodic structures in comparison with previous gap-waveguide-based arrays that deploy signal line and periodic structures on the same substrate [10], [16], [17].

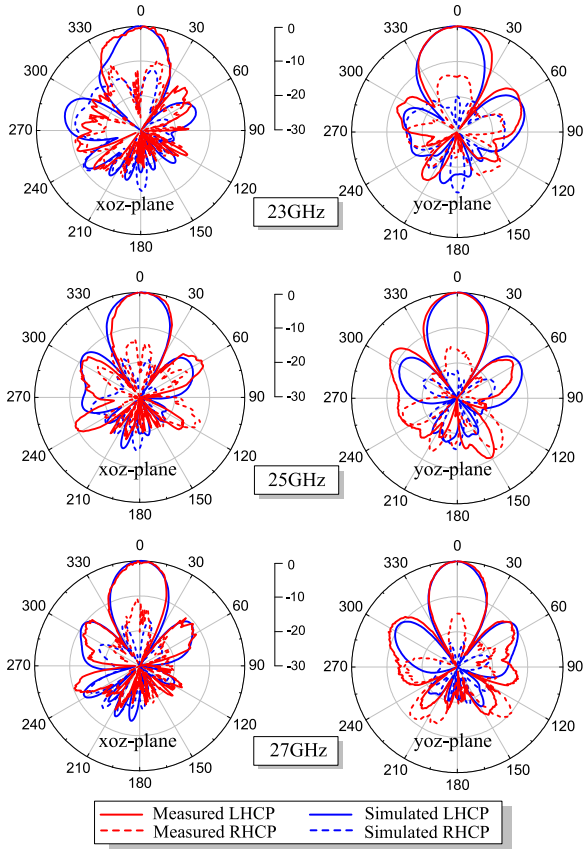

Fig. 9. Measured and simulated CP radiation pattern in *xoz* and *yoz* plane.

TABLE I
COMPARISON TO REPORTED MMW CP ANTENNA ARRAYS

Ref.	Feed Type	Freq. (GHz)	Scale	Impedance BW (%)	3-dB AR BW (%)	Peak Gain (dBic)
[4]	MSL	60	4×4	22.03	18.18	15.98
[5]	MSL (LTCC)	35	2×2	29.6	26	9.3
[8]	SIW	28	2×2	23.3	7.7	10.8
[9]	SIW	60	4×4	14.1	19.4	19.5
[10]	RGW (Metallic)	31	8×8	22	21.8	23.5
This work	SIGW	26	2×2	25.6	19	11.53

IV. CONCLUSION

A single-feed CP patch antenna excited by SIGW has been presented. A truncated-corner patch is placed above SIGW to create the CP radiation, which is driven by a coupling signal from the slot etched on SIGW. In order to improve the AR bandwidth and gain of antenna, a 2×2 antenna array is constructed, using SIGW sequentially phase rotate feed network. The calculation of the initial value of characteristic impedance and guide wavelength is given that can facilitate design. A prototype of the proposed array is experimentally validated. The measured -10 dB impedance bandwidth is 25.6% (22.2–28.8 GHz), the 3 dB AR bandwidth is 19% (22.8–27.6 GHz), and the peak gain is 11.53 dBic.

REFERENCES

[1] P. S. Hall, J. S. Dahele, and H. R. James, "Design principles of sequentially fed, wide bandwidth, circularly polarised microstrip antennas," *Proc. Inst. Elect. Eng.*, Oct. 1989, vol. 136, pp. 381–389.

[2] S.-K. Lin and Y.-C. Lin, "A compact sequential-phase feed using uniform transmission lines for circularly polarized sequential-rotation arrays," *IEEE Trans. Antennas Propag.*, vol. 59, no. 7, pp. 2721–2724, Jul. 2011.

[3] S. X. Ta and I. Park, "Compact wideband circularly polarized patch antenna array using metasurface," *IEEE Antennas Wireless Propag. Lett.*, vol. 16, pp. 1932–1936, 2017.

[4] B. Lee and Y. Yoon, "Low-profile, low-cost, broadband millimeter-wave antenna array for high-data-rate WPAN systems," *IEEE Antennas Wireless Propag. Lett.*, vol. 16, pp. 1957–1960, 2017.

[5] H. Sun, Y.-X. Guo, and Z. Wang, "60-GHz circularly polarized U-slot patch antenna array on LTCC," *IEEE Trans. Antennas Propag.*, vol. 61, no. 1, pp. 430–435, Jan. 2013.

[6] M. Du, Y. Dong, J. Xu, and X. Ding, "35-GHz wideband circularly polarized patch array on LTCC," *IEEE Trans. Antennas Propag.*, vol. 65, no. 6, pp. 3235–3240, Jun. 2017.

[7] Y. Lang, S.-W. Qu, and J.-X. Chen, "Wideband circularly polarized substrate integrated cavity-backed antenna array," *IEEE Antennas Wireless Propag. Lett.*, vol. 13, pp. 1513–1516, 2014.

[8] Q. Wu, H. Wang, C. Yu, and W. Hong, "Low-profile circularly polarized cavity-backed antennas using SIW techniques," *IEEE Trans. Antennas Propag.*, vol. 64, no. 7, pp. 2832–2839, Jul. 2016.

[9] Q. Zhu, K.-B. Ng, and C. H. Chan, "Printed circularly polarized spiral antenna array for millimeter-wave applications," *IEEE Trans. Antennas Propag.*, vol. 65, no. 2, pp. 636–643, Feb. 2017.

[10] M. Akbari, A. Farahbakhsh, and A.-R. Sebak, "Ridge gap waveguide multilevel sequential feeding network for high-gain circularly polarized array antenna," *IEEE Trans. Antennas Propag.*, vol. 67, no. 1, pp. 251–259, Jan. 2019.

[11] J. Zhang, X. Zhang, D. Shen, and A. Kishk, "Design of packaged microstrip line," in *IEEE MTT-S Int. Microw. Symp. Dig.*, San Francisco, CA, USA, May 2016, pp. 1–4.

[12] J. Zhang, X. Zhang, D. Shen, and A. Kishk, "Packaged microstrip line: A new quasi-TEM line for microwave and millimeter-wave applications," *IEEE Trans. Microw. Theory Techn.*, vol. 65, no. 3, pp. 707–719, Mar. 2017.

[13] N. Bayat-Makou and A. A. Kishk, "Millimeter-wave substrate integrated dual level gap waveguide horn antenna," *IEEE Trans. Antennas Propag.*, vol. 65, no. 12, pp. 6847–6855, Dec. 2017.

[14] D. Shen, C. Ma, W. Ren, X. Zhang, Z. Ma, and R. Qian, "A low-profile substrate-integrated-gap-waveguide-fed magnetoelectric dipole," *IEEE Antennas Wireless Propag. Lett.*, vol. 17, no. 18, pp. 1373–1376, Aug. 2018.

[15] Z. N. Chen and M. Y. W. Chia, *Broadband Planar Antennas Design and Applications*. Hoboken, NJ, USA: Wiley, pp. 31–32, 2006.

[16] S. A. Razavi, P. S. Kildal, L. Xiang, E. Alfonso Alos, and H. Chen, "2×2-slot element for 60-GHz planar array antenna realized on two doubledsided PCBs using SIW cavity and EBG-type soft surface fed by microstripridge gap waveguide," *IEEE Trans. Antennas Propag.*, vol. 62, no. 9, pp. 4564–4573, Sep. 2014.

[17] J. Zhang, X. Zhang, and A. A. Kishk, "Broadband 60 GHz antennas fed by substrate integrated gap waveguides," *IEEE Trans. Antennas Propag.*, vol. 66, no. 7, pp. 3261–3270, Jul. 2018.